Chalcogenide Letters Vol. 21, No. 10, October 2024, p. 829 - 839

Prediction of the physics properties of solar material Cu_2BaSnS_4

L. M. Pu [a,*], S. G. Pei [a], X. H. Tang [a], Z. F. Yin [b], H. J. Hou [b], H. L. Guo [c]
[a] *Yancheng KinderGarten Teachers College, Yancheng, 224051, China*
[b] *School of Materials Science and Engineering, Yancheng Institute of Technology, Yancheng, Jiangsu 224051, PR China*
[c] *College of Electronic and Information Engineering, Yangtze Normal University, Fuling, 408000, Chongqing, China*

Recently, there has been a suggestion that Cu_2BaSnS_4 could be a promising candidate for a photovoltaic absorber with a wide band gap. The study primarily examined the structural, along with the mechanical and thermodynamic characteristics of Cu_2BaSnS_4. In addition, a study was performed to examine the presentation and representation of three-dimensional (3D) characteristics related to linear compressibility, shear modulus, and Young's modulus. The investigation into thermodynamic characteristics was calculated and analyzed.

(Received August 11, 2024; Accepted October 21, 2024)

Keywords: Cu_2BaSnS_4, Elastic, Thermodynamic

1. Introduction

Reaching achievements in the advancement of various photoabsorber materials for solar cells has been made possible through the implementation of charge-balanced, multi-component substitutions within II-VI semiconductors[1]. Significantly, Cu(In, Ga)Se_2 (CIGS), a chalcopyrite compound with the composition I-III-VI_2, has achieved significant advancements as a well-established thin-film absorber[2]. Reaching beyond the II-VI structure, the $Cu_2ZnSn(S, Se)_4$ has exhibited efficiencies exceeding 10% [3]. In the field of solar materials, the substitution of Zn with Sr or Ba in $Cu_2ZnSn(S, Se)_4$ is exceptionally captivating. By incorporating selenium, the band gaps of Cu_2BaSnS_4 and Cu_2SrSnS_4 can be adjusted to achieve a wider range suitable for optimizing tandem cell top absorbers, surpassing $Cu_2ZnSn(S, Se)_4$ in terms of band gap width. Cu_2BaSnS_4 and Cu_2SrSnS_4 exhibit wider band gaps than $Cu_2ZnSn(S, Se)_4$. For instance, the synthesis of Cu_2BaSnS_4 and Cu_2SrSnS_4 has been successfully achieved [4]. As we known, the above quaternary compounds demonstrate a structure with trigonal symmetry in the P31 space group. As part of their research, Hong et al. utilized theoretical research to examine the properties of quaternary compounds with a trigonal crystal structure, specifically focusing on the stability and characteristics related to electronics, optics, and defects in Cu_2-II-Sn-VI_4 materials[5]. Experimental and theoretical research the Photoabsorbers Cu_2SrSnS_4 and Cu_2BaSnS_4 has been conducted by Crovetto et al [6]. Inadequate investigations have been conducted on the Cu_2BaSnS_4

* Corresponding author: pulmyct@163.com
https://doi.org/10.15251/CL.2024.2110.829

crystal, despite the existence of numerous reports and data. Therefore, the objective of present work is to conduct a analysis on the structural, elastic, and thermodynamic characteristics of Cu_2BaSnS_4 utilizing a first-principles methodology.

2. Theoretical details

In this study, the crystal structure and mechanical properties of Cu_2BaSnS_4 were determined using the first-principles approach, employing the CASTEP software[7]. The generalized gradient approximation (GGA) method proposed by Perdew-Burke-Ernzerhof (PBE) [8] was utilized to calculate the exchange-correlation potential. Furthermore, a Vanderbilt ultrasoft pseudopotential [9] was utilized for the trigonal structure with a cutoff energy set at 450 eV. The Monkhorst-Pack method was employed to produce a 6×6×2 *k*-point grid for Cu_2BaSnS_4.

3. Results and discussion

3.1. Structural properties

The trigonal structure and space group P31 are adopted by Cu_2BaSnS_4. We assigned the (0, 0, 0) coordinates to Cu atoms, (0, 0, 0.5) coordinates to Ba atoms, and (0.2577, 0.25, 0.125) coordinates to Sn atoms. Fig. 1 shows the crystal structure of Cu_2BaSnS_4. The lattice constants of the Cu_2BaSnS_4 is listed in Table 1. Our obtained lattice constants of Cu_2BaSnS_4 in this study exhibit strong consistency with the experimental findings [10] and theoretical calculations [5, 6]. There might be slight discrepancies in the individual values, but they are within a margin of less than 1%. Therefore, the existing computational method combined with the established variables showcases both possibility and reliability.

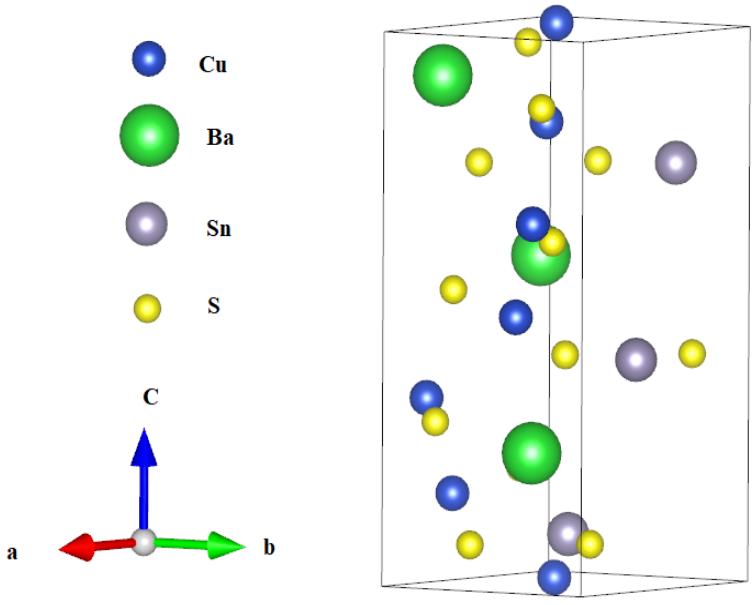

Fig. 1. The structure model of Cu_2BaSnS_4.

Table 1. Calculated lattice constants (a, c) (Å), volume V (Å^3) of Cu_2BaSnS_4.

		a (Å)	*c* (Å)	*V*
Present	GGA-PBE	6.4474	15.8779	571.601
Theo.[5]	PBE	6.450	15.867	571.869
Theo.[5]	GGA+U	6.393	15.852	561.610
Theo.[5]	HSE	6.410	15.862	564.067
Theo.[6]	PBEsol	6.337	15.580	551.64
Theo.[6]	LDA	6.273	15.408	530.944
Theo.[6]	PBE	6.450	15.854	571.201
Exp.[10]		6.367	15.833	555.858

3.2. Elastic properties

To the extent of our comprehension, elastic stiffness tensor of trigonal compounds comprises six unique constituents that can be ascribed to the symmetry characteristics observed within the space group. These components are denoted as C_{11}, C_{33}, C_{44}, C_{12}, C_{13}, and C_{14}. The above elastic compliance tensor components of Cu_2BaSnS_4, obtained through the density functional theory approach, are provided in Table 2. The adherence of the elastic stiffness tensor components to a set of specific relations, referred to as Born stability criteria [11], is required. The values obtained in Table 2 meet all the specified constraints, suggesting that Cu_2BaSnS_4 exhibits mechanical stability. In Table 2, the bulk modulus *B* (GPa), shear modulus *G* (GPa), Young's modulus *E* (GPa), and Poisson's ratio *v* of Cu_2BaSnS_4 are determined using the approximation method proposed by Voigt, Reuss, and Hill [12-14]. The determination of the ductile/brittle can be achieved by considering Poisson's ratio *v*, which represents the ratio between *G*/*B*, as well as Cauchy pressure C_{12}-C_{44}[15, 16]. The material exhibits brittleness when *v* is less than 0.26, *G*/*B* > 0.57, and C_{12}-C_{44} < 0. Otherwise, it exhibits ductility. Table 2 also showcases the ductility characteristics of Cu_2BaSnS_4, as evidenced by its parameters *v*, *G*/*B*, and C_{12}-C_{44}.

Table 2. The calculated elastic constants C_{ij} (GPa), bulk modulus B (GPa), shear modulus G (GPa), Young's modulus E (GPa), G/B, Poisson's ratio v, C_{12}-C_{44} (GPa) and hardness H_V (GPa) of Cu_2BaSnS_4.

C_{11}	C_{33}	C_{44}	C_{12}	C_{13}	C_{14}	*B*	*E*	*G*	*G*/*B*	*v*	C_{12}-C_{44}	H_V^a	H_V^b
81.8	82.7	28.5	32.6	38.1	-1.0	51.5	65.3	25.3	0.49	0.29	4.1	4.04	2.76

(The abbreviation H_V^a represents the hardness model proposed by Chen, while H_V^b refers to the hardness model put forward by Miao)

The parameter of material hardness holds significant importance. In our research, we employed two theoretical frameworks to conduct calculations on the Vickers hardness H_V of trigonal Cu_2BaSnS_4 [17, 18]

$$H_V{}^{a} = 0.92(\frac{G}{B})^{1.137} G^{0.708} \quad (1)$$

$$H_V{}^{b} = 2(\frac{G^3}{B^2})^{0.585} - 3 \quad (2)$$

The successful calculation of material hardness has been achieved using these two theoretical models. As indicated in Table 2, the hardness values of Cu_2BaSnS_4 are approximately 4.04 and 2.76 GPa according to these two respective theoretical models. The consistent results obtained from both approaches affirm the accuracy of our calculations.

Moreover, it is possible to theoretically calculate thermal properties by employing the elastic coefficients and moduli. Hence, we perform computations to ascertain the sound velocities of Cu_2BaSnS_4 by utilizing the provided equations [19].

$$v_t = (\frac{G}{\rho})^{1/2} \quad (3)$$

$$v_l = [(B + \frac{4G}{3}) / \rho]^{1/2} \quad (4)$$

$$v_m = [\frac{1}{3}(\frac{2}{v_t^3} + \frac{1}{v_l^3})]^{-1/3} \quad (5)$$

The longitudinal, transverse, and average sound velocities are denoted as v_l, v_t, and v_m, correspondingly. The density of trigonal Cu_2BaSnS_4 is represented by ρ. By utilizing the v_m, it becomes possible to determine the Debye temperature using the following approach [20]

$$\theta = \frac{h}{k_B}[\frac{3n}{4\pi}(\frac{NA\rho}{M})]^{1/3} v_m \quad (6)$$

n is the total number of trigonal Cu_2BaSnS_4 atoms in each unit cell. M is the molecular weight.

Furthermore, it is possible to determine the thermal conductivity κ through the utilization of the equations[21]

$$\kappa_{\min} = 0.87 k_B M a^{-\frac{2}{3}} \rho^{\frac{1}{6}} E^{\frac{1}{2}} \quad (7)$$

Here, k_B is Boltzmann's constant, ρ is the density, M_a is the average mass per atom, respectively. Table 3 displays the v_l, v_t, v_m, θ, and k acquired for Cu_2BaSnS_4. Regrettably, there is a lack of empirical and theoretical evidence available for comparison.

Table 3. Calculated the density ρ (g/cm³), v_l, v_t, v_m) (km/s), θ (K) and k (W.m⁻¹K⁻¹) of trigonal Cu_2BaSnS_4.

	ρ	v_l	v_t	v_m	θ	k
Trigonal-Cu_2BaSnS_4	4.459	4.37	2.381	2.6568	274.9	0.5553

The determination of anisotropic elasticity in a specific orientation, encompassing the linear compressibility β, G, and E, can be achieved by utilizing formulas that integrate the elastic compliance constants S_{ij} and direction cosines (l_1, l_2, and l_3)[22]

For trigonal structure

$$\beta = (S_{11} + S_{12} + S_{13}) - (S_{11} + S_{12} - S_{13} - S_{33})l_3^2 \tag{8}$$

$$\begin{aligned}\frac{1}{G_t} &= S_{11}(3l_1^2 + 3l_2^2 - 2l_1^4 - 2l_2^4 - 4l_1^2l_1^2) + 2S_{33}l_3^2(1 - l_3^2) \\ &+ \frac{1}{2}S_{44}(l_1^2 + l_2^2 + 2l_3^2 - 4l_2^2l_3^2 - 4l_1^2l_3^2) - S_{12}(l_1^2 + l_2^2) \\ &-4S_{13}l_3^2(l_1^2 + l_3^2) + 2S_{14}(2l_2^3l_3 - 5l_1^2l_2l_3 - l_2^2l_1l_3)\end{aligned} \tag{9}$$

$$\frac{1}{E} = (1 - l_3^2)^2 S_{11} + l_3^4 S_{33} + l_3^2(1 - l_3^2)(2S_{13} + S_{44}) + 2S_{14}l_2l_3(3l_1^2 - l_2^2) \tag{10}$$

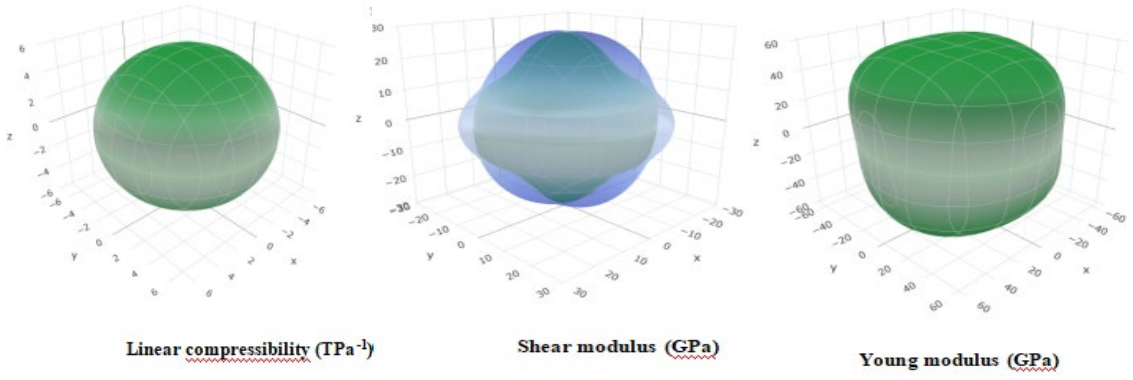

Fig. 2. A three-dimensional (3D) surface contours of β, E, and G of Cu_2BaSnS_4.

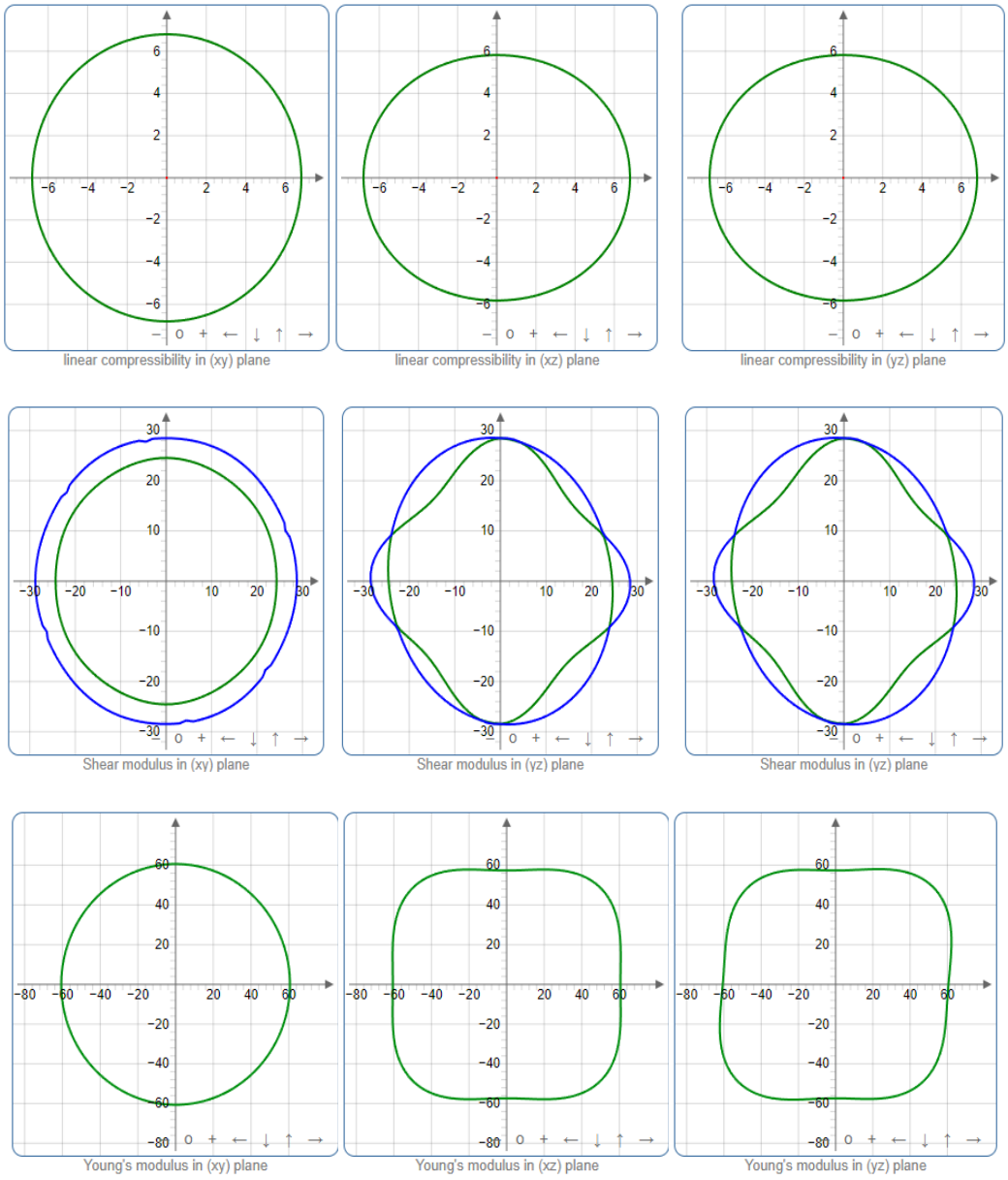

Fig. 3. Projections of β, E, and G *in different planes of* Cu_2BaSnS_4.

The graphical depictions of β, E, and G in different planes and 3D formats play a crucial role in visually demonstrating the crystal's elastic anisotropy. These matrices are input into the ELATE software [22-24]. Fig. 2-3 displays the direction dependence of β, G and E of Cu_2BaSnS_4 in different planes (xy-, xz-, and yz-planes) and 3D perspectives. It should be noted that the presence of a spherical 3D surface structure in a material indicates isotropy, while any departure from this feature implies anisotropy. As illustrated in Fig. 2, the anisotropy of E, β, and G can be attributed to their non-spherical characteristics. Fig. 3 exhibits the representation of elastic moduli for trigonal-Cu_2BaSnS_4 on the different planes. In the meantime, a analysis was carried out to determine the anisotropy of Cu_2BaSnS_4 by evaluating ratios such as β_{max}/β_{min}, G_{max}/G_{min}, and E_{max}/E_{min}. Larger anisotropy can be inferred from higher ratio values. According to representation

in different planes and 3D formats graphical plots indicate that the anisotropy sequence in Cu_2BaSnS_4 is $G > E > \beta$.

3.3. Thermodynamic properties

The subject of condensed matter physics presents an intriguing exploration into the thermodynamic characteristics exhibited by solid materials under pressures and temperatures. To investigate the influence of pressure (temperature) on these thermodynamic characteristics, we utilize the quasi-harmonic Debye method [25]. We employed a range of crystal parameters to derive the *E-V* data, which represents the total energy *E* and volume *V* as depicted in Fig. 6. Furthermore, thermodynamic properties were derived from *E-V* data and a quasi-harmonic Debye modeling approach was employed. The estimation of the bulk modulus *B* as 59.05 GPa, along with its pressure derivative of B' = 4.89, was obtained from Birch-Murnaghan's equation of state[26]. Our calculations exhibit a high level of concurrence with the theoretical outcome *B* = 51.5 GPa.

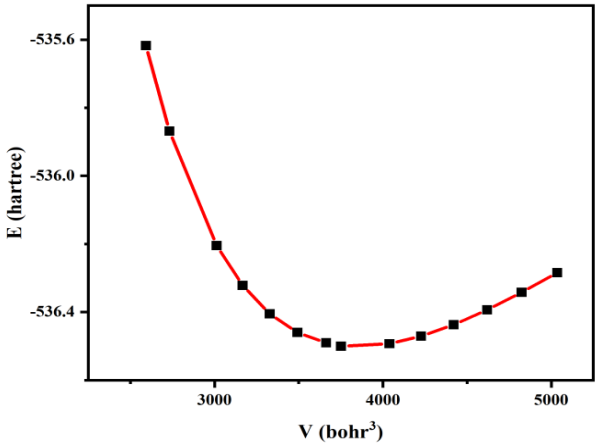

Fig. 4. Energy E change with volume V.

Fig. 5 illustrates the *B* change with temperature at (0, 4, 8GPa). Under a constant pressure, *B* exhibits a decreasing trend with increasing *T*. Similarly, under a constant temperature, *B* demonstrates an increasing pattern as *T* rises. A rise in *P* leads to a proportional rise in *B* under constant temperature conditions. For a constant pressure, the *B* decreases as *T* increases. The size of the *B* curve can be adjusted to achieve an equivalent outcome. It is feasible to either enhance *P* or reduce *T* in order to attain an equivalent outcome for the substance.

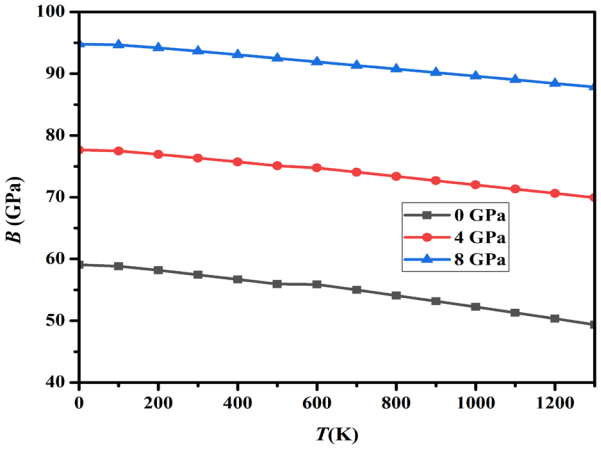

Fig. 5. Bulk modulus B change with temperature at (0, 4, 8GPa) of Cu_2BaSnS_4.

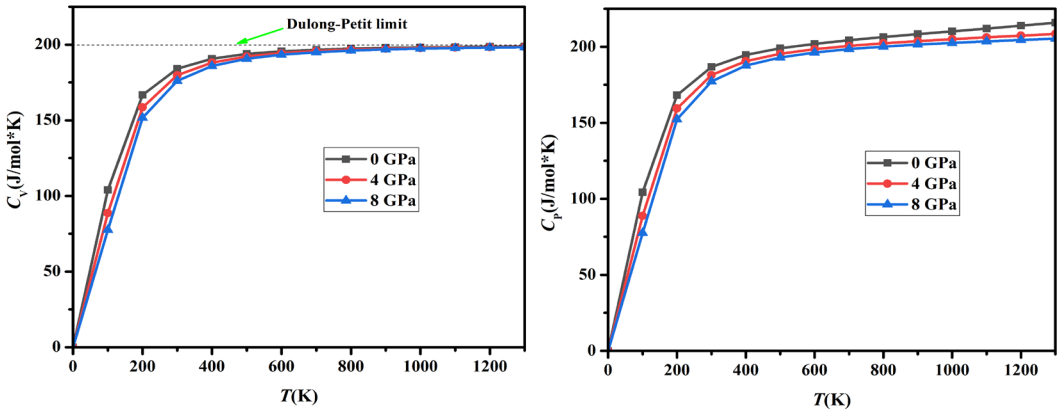

Fig. 6. C_V and C_P change with temperature at (0, 4, 8 GPa) of Cu_2BaSnS_4.

Fig. 6(a) illustrates the C_V change with temperature at (0, 4, 8GPa) of Cu_2BaSnS_4, as determined through calculations. It is evident from the data presented in Fig. 6(a) that, for temperatures below 500 K, there is a significant exponential growth observed in the heat capacity C_V as temperature increases. However, at elevated temperatures, it adheres to the Dulong-Petit limit. In addition, the heat capacity C_V exhibits a noticeable similarity in its increased tendency at different pressure. Fig. 6(b) depicts the correlation between heat capacity and pressure across different temperature levels. Our analysis indicates that the heat capacity C_P exhibits contrasting responses to variations in temperature and pressure. In particular, a rise in temperature causes C_P to increase, whereas an elevation in pressure leads to a reduction in C_P. Furthermore, it is noteworthy that the impact of temperature on C_P is more pronounced compared to that of pressure.

α change with temperature T at P = 0, 4 and 8 GPa is plotted in Fig. 7. The α tends to exhibit a predominantly exponential growth as the temperature T increases, while maintaining a fixed pressure P. It can be observed that the impact of temperature on the α is more significant at elevated temperatures (T) compared to lower temperatures (T).

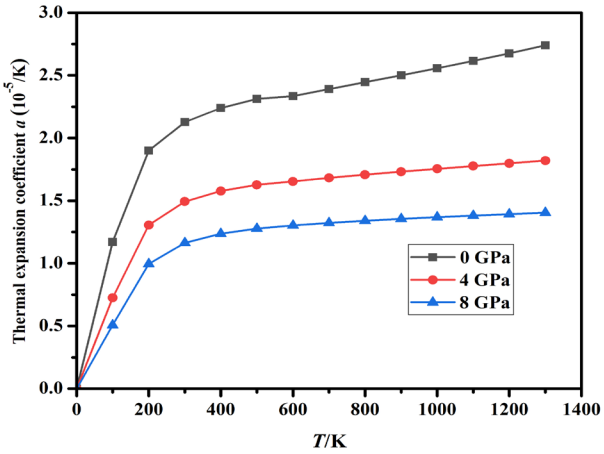

Fig. 7. α change with temperature T at P = 0, 4 and 8 GPa, respectively.

*Table 4. The calculated S (J/mol*K), θ (K), γ for Cu_2BaSnS_4 at 100, 500, 800 and 1100 K under (0, 2,4, 6, 8, 10 GPa).*

T/K	*P*/GPa	0	2	4	6	8	10
100	*S*	55.191	48.214	42.872	38.642	35.179	32.174
	θ	387.87	415.93	440.73	463.02	483.46	503.18
	γ	2.284	2.157	2.060	1.983	1.919	1.862
500	*S*	323.308	308.996	297.342	287.505	278.994	271.270
	θ	380.73	409.97	435.54	458.46	479.34	499.20
	γ	2.320	2.182	2.079	1.998	1.931	1.873
800	*S*	417.764	403.321	390.700	380.272	371.567	363.509
	θ	376.12	404.70	431.50	455.01	475.65	495.62
	γ	2.344	2.205	2.095	2.010	1.943	1.884
1100	*S*	484.765	468.988	455.890	445.027	435.887	427.627
	θ	368.67	399.19	426.47	450.52	471.83	491.96
	γ	2.384	2.230	2.114	2.025	1.955	1.894

In addition, we have conducted calculations to determine the *S*, *θ*, and *γ* of Cu_2BaSnS_4 under conditions of elevated temperature and pressure. The outcomes obtained are displayed in Table 4. We have conducted calculations to determine the thermodynamic properties of Cu_2BaSnS_4, as there is a lack of available data on its measurements under high temperature and pressure conditions. Hence, our findings serve as valuable contributions in providing insights into the thermodynamic behavior of Cu_2BaSnS_4.

4. Conclusions

We employ a theoretical method to computationally the structural, elastic anisotropy and thermal properties of Cu_2BaSnS_4. The structural parameters of Cu_2BaSnS_4 have been successfully determined. The mechanical stability of Cu_2BaSnS_4 is found to be highly favorable based on the criteria. Based on the determined C_{ij} values for elasticity constants, a range of physical parameters can be obtained to characterize the mechanical characteristics of Cu_2BaSnS_4, including B, G, E, and more. The thermodynamic properties of Cu_2BaSnS_4 is studied in conjunction with the quasi-harmonic Debye model.

References

[1] B. R. Pamplin, J. Phys. Chem. Solids 25(1964) 675-684; https://doi.org/10.1016/0022-3697(64)90176-3

[2] C. Wang, S.Chen, J. H.Yang, L. Lang, H. J.Xiang, X.G. Gong, A. Walsh, S.H. Wei, Chem. Mater. 26(2014)3411-3417; https://doi.org/10.1021/cm500598x

[3] M. A. Green, E. D. Dunlop, J. Hohl-Ebinger, M. Yoshita, N. Kopidakis, A. W. Y. Ho-Baillie, Prog. Photovoltaics 28(2020)3-15; https://doi.org/10.1002/pip.3171

[4] A. Assoud, N. Soheilnia, H. Kleinke, Properties Chem. Mater. 17 (2005)2255-2261; https://doi.org/10.1021/cm050102u

[5] F. Hong, W. J. Lin, W.W. Meng, Y.F. Yan, Phys. Chem. Chem. Phys.18(2016)4828; https://doi.org/10.1039/c5cp06977g

[6] A. Crovetto, Z.D. Xing, M. Fischer, R. Nielsen, C. N. Savory, T. Rindzevicius, N. Stenger, D. O. Scanlon, Ib Chorkendorff, Peter C. K. Vesborg, ACS Appl. Mater. Interfaces 12(2020)50446-50454; https://doi.org/10.1021/acsami.0c14578

[7] M. D. Segall, P. J. D. Lindan, M. J. Probert, C. J. Pickard, P.J. Hasnip, S. J. Clark, M.C. Payne, J. Phys. Condens. Mater. 14 (2002) 2717; https://doi.org/10.1088/0953-8984/14/11/301

[8] J. P.Perdew, K. Burke, M. Ernzerhof, Phys. Rev. Lett. 77(1996) 3865; https://doi.org/10.1103/PhysRevLett.77.3865

[9] D. Vanderbilt, Phys. Rev. B 41 (1990) 7892; https://doi.org/10.1103/PhysRevB.41.7892

[10] C. L. Teske, O. Vetter, Z. Anorg. Allg. Chem., 426 (1976)281-287; https://doi.org/10.1002/zaac.19764260308

[11] M. Born, K. Huang, Dynamical Theory of Crystal Lattices (Oxford: Clarendon) 1954.

[12] W. Voigt, Handbook of Crystal Physics, Taubner, Leipzig, 1928.

[13] A. Reuss, Z. Angew. Math. Mech 9(1929) 49; https://doi.org/10.1002/zamm.19290090104

[14] R. Hill, Proceedings of the Physical Society. Section A, 1952, 65(5): 349; https://doi.org/10.1088/0370-1298/65/5/307

[15] S. F. Pugh, Philos. Mag. 45, 823 (1954); https://doi.org/10.1080/14786440808520496

[16] D.G. Pettifor, Mater. Sci. Technol. 8 (1992) 345-349; https://doi.org/10.1179/mst.1992.8.4.345

[17] Y. Tian, B. Xu, Z. Zhao, Int. J. Refract. Met. Hard Mater. 33 (2012) 93-106; https://doi.org/10.1016/j.ijrmhm.2012.02.021

[18] S. Chen, Y. Sun, Y.H. Duan, B. Huang, M.J. Peng, J. Alloy. Compd. 630 (2015) 202-208; https://doi.org/10.1016/j.jallcom.2015.01.038

[19] D. Music, A. Houben, R. Dronskowski, J.M. Schneider, Phys. Rev. B 75 (2007) 174102; http://dx.doi.org/10.1103/PhysRevB.75.174102

[20] M. A. Ali, M. M. Hossain, M.M. Uddin, M.A. Hossain, A.K.M.A. Islam, S.H. Naqib, J. Mater. Res. Techno.11(2021)1000; https://doi.org/10.1016/j.jmrt.2021.01.068

[21] M. Born, K. Huang 1954 Dynamical Theory of Crystal Lattices (Oxford: Clarendon)

[22] R. Gaillac, P. Pullumbi, F. X.Coudert, Journal of Physics: Condensed Matter, 28 (2016) 275201; https://doi.org/10.1088/0953-8984/28/27/275201

[23] Q. Fan, S. R. Zhang, H. J. Hou, J. H. Yang, Vacuum 208 (2023) 111648; https://doi.org/10.1016/j.vacuum.2022.111648

[24] H.J. Hou, W.X. Chen, L.X. Xiao, H.Y. Wang, H.J. Zhu, X.W. Lu, S.R. Zhang, H.L. Guo, Q.F. Zhang, Vacuum 213 (2023) 112136; https://doi.org/10.1016/j.vacuum.2023.112136

[25] M.A. Blanco, E. Francisco, V. Luana, Comput. Phys. Comm. 158 (2004)57-72; https://doi.org/10.1016/j.comphy.2003.12.001

[26] F.D. Murnaghan, Proc. Nat. Acad. Sci. USA 30 (1944) 244; https://doi.org/10.1073/pnas.30.9.244